ORIGINAL PAPER - CONDENSED MATTER

Co-sensitization effect of chlorophyll and anthocyanin on optical absorption properties and power conversion efficiency of dye-sensitized solar cells

Emma Panzi Mukhokosi[1] · Tibenkana Mohammed[1] · Namanya Loyce[1] · Nandipha L. Botha[2,3] · Maliki Maaza[2,3] · Dhayalan Velauthapillai[4]

Abstract

In this article, the chemical structure, optical absorption and photoluminescence properties of un/adsorbed dyes of hibiscus flower (H), pumpkin leaf (P), sweet potato leaf (S) and their composites (H: P & H: S) have been studied. The chemical structural properties revealed the O–H, C–C and C=O as the main anchoring functional groups. The optical absorption properties revealed two definite bands in between 450–500 nm and 600–680 nm wavelength for chlorophyll-based dyes and a peak at 526 nm for anthocyanin based dye extract. The composite dye extracts revealed optical absorption bands corresponding to chlorophyll and anthocyanin pigments with enhanced absorption of light. Five different solar cells based on H, P, S, H:P-3:1 and H:S-3:1 were developed and revealed an efficiency of ∼ 0.08, 0.3, 0.5, 0.7 and ∼ 1% respectively. The efficiency was reduced by half after 30 days. The composites had the highest power conversion efficiency due to more O–H, C–C and C=O binding sites on TiO_2 nanoparticles, reduced rate of electron–hole pair recombination and a wide range of optical absorption. These studies suggest that co-pigmentation can be an alternative strategy to increasing the power conversion efficiency in DSSCs.

Keywords Chlorophyll · Anthocyanin · Co-sensitizer · DSSCs · Photoluminescence

1 Introduction

Renewable energy from sun light is an alternative to non-renewable energy sources. It is clean, inexhaustible, easy to access and abundant energy resource on the surface of the earth [1]. Third generational solar cells like dye sensitized solar cells (DSSCs) have attracted attention in the research community because of the ease of processing and abundance of plant based dye extracts [2]. A DSSC has a similar working mechanism like a photo-electrochemical cell, where the production and movement of electrons are influenced by the interaction of chemical reactions and photon energy. The schematic diagram of a DSSC is shown in Fig. 1. The structure is basically comprised of four components; the dye (sensitizer), mesoporous photo-anode with a semi-conducting layer usually TiO_2, liquid electrolyte usually (e.g. iodide/ triiodide, I^-/I_3^-), and counter electrode (CE) usually Platinum (Pt). The thin films of semiconducting photo-anode and the Pt counter electrode materials are usually coated on transparent conductive oxide glass substrates (TCO). The most common substrates used are fluorine-doped glass substrates (FTO) and indium doped glass substrates (ITO). The latter is widely used not only in DSSCs but other electronic/optoelectronic devices[3]. The internal processes that take place inside a dye sensitized solar cell have been explained elsewhere in literature [3–5].

The efficiency of solar cells is calculated based on the relation [6].

✉ Emma Panzi Mukhokosi
panzi2018@gmail.com; epmukhokosi@kyu.ac.ug

1 Department of Physics, Faculty of Science, Kyambogo University, PO Box 1, Kyambogo, Uganda

2 College of Graduate Studies, UNESCO UNISA Africa Chair in Nanosciences and Nanotechnology, University of South Africa, PO Box 392, Pretoria, South Africa

3 Materials Research Department, Nanosciences African Network (NANOAFNET), iThemba LABS, PO Box 722, Cape Town, South Africa

4 Faculty of Engineering and Science, Western Norway University of Applied Sciences, 5063 Bergen, Norway
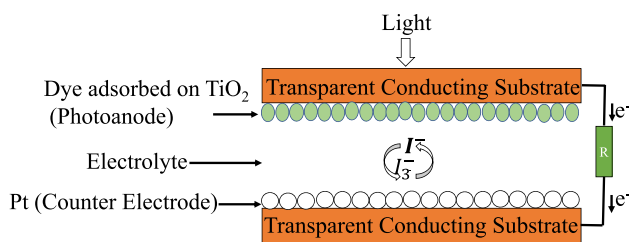
Fig. 1 A schematic diagram of a DSSCs

$$\eta = \frac{V_{oc}J_{sc}FF}{P_{in}} = \frac{P_{max}}{P_{in}}. \tag{1}$$

Here V_{oc} is the open-circuit voltage, J_{sc} is short-circuit current density, FF is the fill factor, P_{max}, is the maximum power generated by the device and P_{in} is the incident photon power [7]. In DSSCs, sensitizing dye is a crucial component. Dyes based on ruthenium (II) and osmium (II) complexes have been found to be the most efficient with an efficiency of over 13% [8]. Despite of that, they are costly, have heavy metals which have negative effects on the environment and are associated with complicated synthesis procedures [7]. Natural dyes are an alternative to the synthetic dyes due to their abundance, simple preparation procedures, and biodegradability [9]. Plant-based dyes extracted from leaves, roots, tree barks, flowers and their composites (co-pigmentation) have been performed by various researchers, although these devices suffer from low levels efficiency and short-term stability as compared to synthetic dyes [3, 9–12]. Therefore, alternate dyes extracted from other plant based materials and their combinations (co-pigmentation) need to be studied extensively in order to improve on their photovoltaic efficiency and evaluate on their long term stability for potential industrial production. Pumpkin leafs (chlorophyll pigment), sweet potato leafs (Chlorophyll pigment) and hibiscus flowers (anthocyanin pigment) are non-perennial and perennial plants respectively, abundant and non-toxic. They are widely cultivated in Uganda, used as food (pumpkin leafs), beverages (hibiscus flower) and animal feeds (sweet potato leafs). The dye extracts from these plant materials and their composites have not been studied as dye sensitizers in DSSCs. In this article, we extracted dyes from pumpkin leafs, sweet potato leafs, hibiscus flowers and their composites as potential sensitizers in DSSCs. We studied their chemical structural properties, optical absorption properties, photoluminescence properties, fabricated the DSSCs and evaluated their efficiencies. It has been found that the efficiency of the composite dyes is 1% higher than that of the individual dyes and has been attributed to more O–H, C–C and C=O binding sites onto TiO$_2$ nanoparticles, reduced rate of electron–hole pair recombination and a wide wavelength range of optical absorption. The enhanced efficiency has been supported by the decrease in the photoluminescence emission spectra peaks for the adsorbed dyes onto TiO$_2$ nanoparticles. The device efficiencies were reduced by half of the original value after 30 days. These studies suggest that co-pigmentation can be an alternative strategy to increasing the power conversion efficiency in DSSCs.

2 Experimental

2.1 Materials for dye extraction

The materials for dye extraction were pumpkin leafs, sweet potato leafs, hibiscus flowers, distilled water, Whatman filter paper (Cat No 1001 125) and ethanol. The plant leafs were collected from Uganda flora. Ethanol of 96% purity was purchased from Griffchem.

2.2 Extraction of dyes from single plant materials

The plant materials were washed with distilled water and dried at 60 °C in an oven for 24 h. Using a mortar and pestle, the plant materials were then crushed into powdered. 20 g of pumpkin powder was dispersed in 100 ml of ethanol in amber bottle to give a concentration of 0.2 g/ml. Similar procedures were followed for dye extraction from sweet potato leaves and hibiscus powder. The solutions were kept in amber bottles in a dark environment at room temperature for 24 h. Due to the complexity of extracting dye solutions from hibiscus, the solution was warmed at 60 °C in an incubator set at 150 rpm for 10 min and then kept in an amber bottle in a dark environment for a week. The solutions were then filtered and stored in amber bottles in a dark environment for characterization.

2.3 Extraction of dyes from composites

Denoting P as dye extract from pumpkin leaf powder, S as dye extract from sweet potato leaf powder and H as dye extract from hibiscus flower powder, the composites were developed using mass ratios of 3:1 where 3 is for H and 1 is either for P or S. The choice of mass ratios was based on related studies from literature [9, 13]. 20 g of the mass ratio was dissolved in 100 ml of ethanol to give a concentration of 0.2 g/ml. Similar procedures in extraction of dyes from single plant materials discussed in the section above were followed for extraction of composites.

2.4 Materials for photo-anode and counter electrode

The materials used for photo-anode and counter electrode were fluorine doped tin oxide substrates (FTO-2.5×2.5 cm^2)

of sheet resistance $= 6.7 \pm 0.27$ Ω/square cm from Ossila Ltd-UK, TiO_2 powder of particle size < 25 nm (anatase phase) from Sigma Aldrich, dihydrogen hexachloroplatinate (IV) hexahydrate (37.5% Pt, thermos scientific).

2.5 Substrate cleaning

FTO glass substrates were cleaned by soaking them in de-ionized water followed by ethanol. It was then sonicated for 3 h in an alcoholic solution containing de-ionized water and ethanol. They were then removed and allowed to dry in a clean environment at room temperature.

2.6 Preparation of photo-anode and counter electrodes

TiO_2 paste was prepared following previous procedures [2]. In brief, 1 g of TiO_2 nanoparticle were dissolved in 0.3 g of polyethylene glycol having a mixture of glacial acetic acid and de-ionized water of 6 ml each. The resultant mixture was placed in an ultrasonic bath and sonicated for 3 h. Two edges of FTO substrate were sealed using one layer of scotch tape of 0.06 mm in thickness. TiO_2 paste was drop casted five times using a micro-pipette on the substrate and kept at room temperature in a clean environment for 24 h to evaporate the solvent. The thickness of the scotch tape was equivalent to the thin film thickness and the coverage area was 2×2 cm^2. The scotch tape was removed and the film annealed at 300 °C in a muffle furnace for 1 h. The furnace was allowed to cool down naturally and the thin film was removed. The TiO_2 thin film was then immersed in the dye extracts for 24 h. The soaked film was removed from the dye extracts, rinsed with ethanol and then applied as a photo-anode. The platinum counter electrode was prepared by dissolving 40 mg of dihydrogen hexachloroplatinate (IV) hexahydrate in 10 ml of ethanol and stirred on a magnetic plate for 5 min. Five drops were drop casted on FTO substrate using a micro-pipette, kept for 24 h in a clean environment to evaporate the solvent and then annealed at 300 °C for 30 min in a muffle furnace. In total, five photo-anodes and counter electrodes were prepared following the same procedures.

2.7 Characterization of dye extracts, dye co-pigments, TiO_2 nanoparticles and dyes adsorbed on TiO_2 nanoparticles

The chemical structural properties (functional groups) and optical absorption properties of dyes of pumpkin leafs, sweet potato leafs, hibiscus flower and their composites were characterized using Fourier Transform Infrared (FTIR) spectroscopy (SHIMADZU) using KBr pellet and GENESYS 10S UV–Visible spectroscopy (Thermo Scientific) respectively. The absorption spectra were carried out in wavelength range

from 190 to 900 nm. The surface morphology of TiO_2 nanoparticles were characterized using a Scanning Electron Microscope (SEM) and have been reported in our previous publication[2], the particle size of TiO_2 nanoparticles was 12 ± 2 nm determined using Transmission Electron Microscope (TEM), Raman spectroscopy for crystal structural properties of TiO_2 before and after dye adsorption are similarly reported in our previous studies[2]. Photoluminescence spectra was characterized using an FL spectrometer with an ocean optics system (350 nm UV light emitting diode). The surface morphology of the dyes adsorbed on TiO_2 nanoparticles were investigated by a scanning electron microscope (FESEM, Jeol JSM-7400F).

2.8 Preparation of the electrolyte

Here, 0.127 g of iodine (I_2) and 0.83 g of potassium iodide were placed into a clean beaker containing 10 ml of ethylene glycol, stirred for 30 min and stored in amber bottle [14].

2.9 Assembly of the DSSCs and current–voltage (I-V) measurements

After dye adsorption, the photo-anode and counter electrodes were sandwiched in such that conductive sides face each other. The electrolyte was drop casted at the edges of the substrates and drawn into the space between the electrodes by capillary action. Using binder clips, the electrodes were firmly held together. Under one sun (AM1.5 100 mWcm^{-2}) illumination from a solar simulator, the performance of the solar cells was evaluated and the *I-V* characteristic were recorded using Keithley SMU-2450. The active area of the device was 2 cm^2.

3 Results and discussion

3.1 Optical absorption properties of individual dye extracts and their composite

The UV–Vis spectra was used to characterize the optical absorption characteristics of the extracted dyes and determine their potential to absorb and convert the suns photon energy into electrical power. The spectra of the extracted dyes at different dye concentrations from hibiscus flower, sweet potato leaf and pumpkin leaf are shown in Fig. 2. Figure 2a shows the UV–visible absorbance spectra of hibiscus flower dye extract. There was no significant change in the shape of the peaks with reducing dye concentrations. However, there was reduction in absorbance with reducing dye concentration. This can be attributed to reduction in anthocyanin- anthocyanin interactions. The maximum absorption peak is observed at 526 nm (2.35 eV). This peak signifies
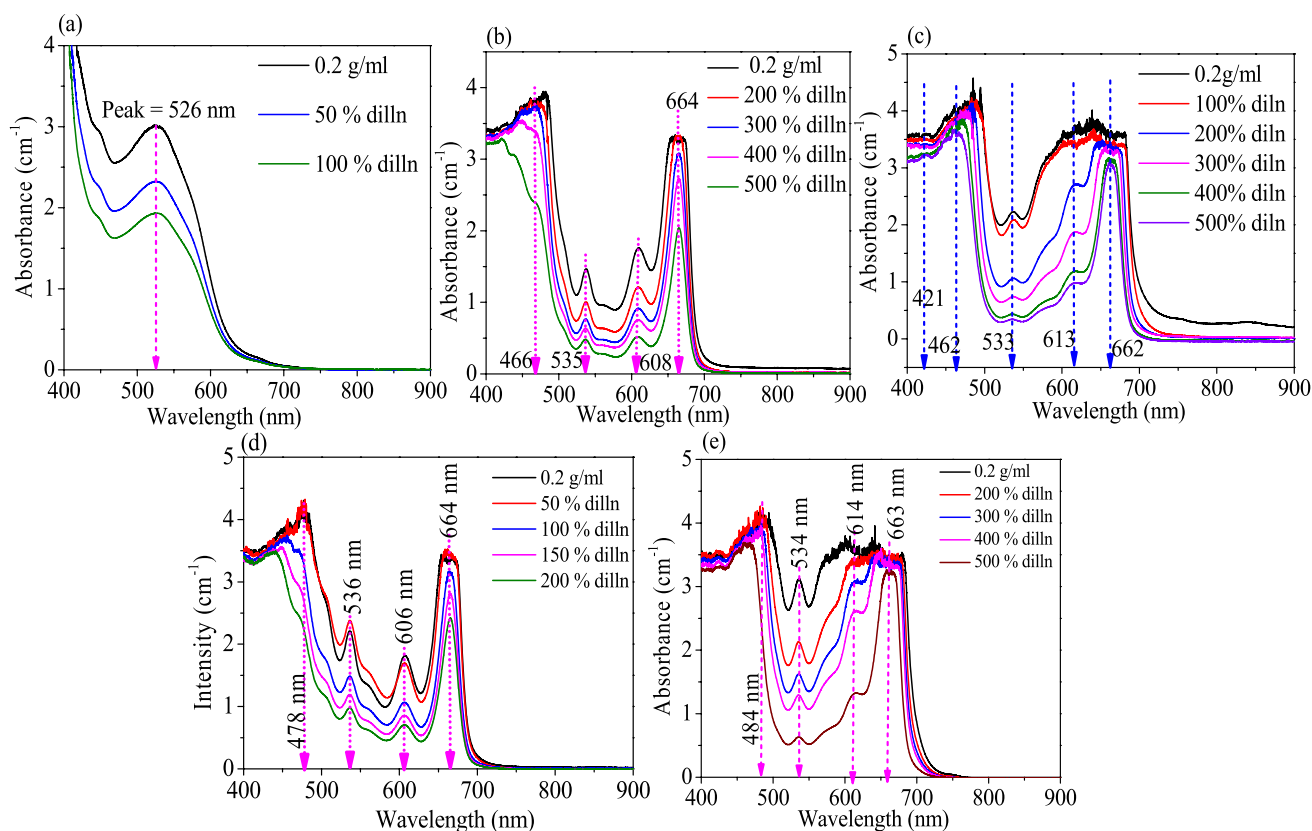
Fig. 2 **a–c** Absorption spectra for hibiscus flower dye extract, sweet potato leaf dye extract and pumpkin leaf dye extract at different dye concentrations, **d** Absorption spectra of sweet potato and Hibiscus flower composite dye extract (S:H-1:3), **e** Absorption spectra of pumpkin leaf and Hibiscus flower composite dye extract (P:H-1:3). Figure **c** was reproduced with permission from reference [2]. NOTE: dilln stands for dilution of the initial concentration with ethanol

that green and adjacent colours are absorbed and red colour in hibiscus is reflected hence presence of anthocyanin pigment in hibiscus. The absorption peak obtained is in the absorption ranges for solar energy applications and in agreement with earlier reports [15–17]. Figure 2b shows the optical absorption properties of sweet potato leaf dye extracts. Two prominent maximum absorption peaks at 466 (2.66 eV) and 664 nm (1.87 eV) are observed. The peak at 466 nm is known as the "blue" (Soret or B-) band and the peak at 664 nm is known as the "red" (Q-) band [18, 19]. The two peaks indicates the presence of Chlorophyll b and a, respectively [2, 19, 20]. Figure 2c shows the absorption spectra of pumpkin leaf dye extract with two major characteristic absorption bands between in the blue-visible region (450–500 nm) or (2.75–2.48 eV) and visible-red region (635–674 nm) or (1.95–1.84 eV), respectively. These two prominent absorption bands indicate the presence of carotenoids (neoxanthin) or chlorophyll b and chlorophyll a, respectively [2, 19–21]. Further, the two sharp absorption peaks at 535 nm (2.32 eV) and 608 nm (2.04 eV) represent the presence of π–π* electronic transitions of the porphyrin ring. The presence of the porphyrin ring confirms the ability of the dye to eject charge

carriers from the excited state of pumpkin leaf sensitizer into the conduction band of TiO_2 photo-anode [21, 22]. Figure 2d and e shows the absorption spectra of the dye composites of sweet potato leaf and Hibiscus flower and pumpkin leaf and hibiscus flower, respectively. It can be observed that there is an increased optical absorption especially in the green region of the spectra which was previously reflected by single chlorophyll dyes, thus, widening the suns photon absorption spectra range for hibiscus pigment. The increased optical absorption is attributed to presence of anthocyanin pigment in the dye composites. It can also be observed that, there is a red shift from about 661 nm to between 663 and 665 nm, a difference of 2–4 nm. The red shift could be due to anthocyanin and chlorophyll interaction. In both pumpkin and sweet potato dye extracts and their composites and at higher concentrations, there was peak broadening of the bands between 600 and 700 nm wavelength range. This broadening of the bands is an indication of chlorophyll-chlorophyll interactions and the aggregation of pheophytin or the existence of two pigments [21, 22]. For lower concentrations, clear, sharp absorption peaks were observed in the spectra. It can be noted that different dilutions factors were

used to optimize the concentration and eliminate the degree of possible dye extract aggregations in the solvent. In general, the ability of the selected dyes and their composites to absorb photon energy across the entire UV–Vis–near infrared spectrum depicts their potential applications as photon absorbers in dye sensitized solar cells.

## 3.2 Fourier Transform Infrared (FTIR) analysis

FTIR spectroscopy is a non-destructive technique that is used to determine the functional groups in chemical compounds found in materials on the basis of peak positions. Ideal dyes are expected to have carboxyl (COOH) or hydroxyl (O–H) anchoring groups that enables them to be adsorbed onto the TiO_2 photo-electrode and are responsible for efficient charge transfer of electrons into the conduction band of the photo-anode and solar cell efficiency [21, 23]. The FTIR spectra of individual and mixed dyes P, S, H, PH, and SH were taken within the range of 4000–500 cm^{-1} and are shown in Fig. 3a. All the dyes have a broad band between 3600 and 3200 cm^{-1} and is due to O–H stretching bond in phenolic compounds with a peak located ~ 3278 cm^{-1} [13, 21, 24]. The peaks located at 2848 and 2915 cm^{-1} correspond to the stretching vibrations of the symmetric (-CH_2) and asymmetric (-CH_3) groups, respectively [9, 25]. The vibration stretching at 1613 cm^{-1} correspond to -C = C of the alkene group [13, 25]. The diminished peak located at 1381 cm^{-1} correspond to C–H bending vibration of CH_3 or alkane group [21]. The diminished vibration peak located at 1312 cm^{-1} correspond to O–H bending vibration of phenols or amide III vibration and the CH_2 wagging modes [21]. The vibration band located at 1240 cm^{-1} correspond to C–O stretching vibration of the alkoxy groups [21]. Further, the presence of functional groups with peaks observed in the dye extracts at 3278, 2915, 1613, 1381, 1312, and 1240 cm^{-1} wavenumbers indicates that the dye extracts can bound effectively with TiO_2 nanoparticles and increase the

electrons transfer process between the dye extracts and TiO_2 layer, which increases short circuit current and power conversion efficiency of the DSSC [18, 26]. It is observed that the transmittance intensities of the composites are higher as compared to the transmittance intensities of individual dyes. The higher intensities can be attributed to the higher mass percentage of anthocyanin present in the dyes. The high mass ratio increases the molecular weight, increasing more anchoring O–H groups that increases the binding sites onto the photo-anode and hence expected to increase the efficiency of the DSSC. From the FTIR spectra of the selected dyes and their composites, it is observed the anchoring group located at 2915 cm^{-1} and 2848 cm^{-1} in S:H-1:3 (corresponding to C–H stretching vibrations of methyl (CH_3) and methylene (CH_2) group) have the highest transmittance intensities as compared with other dyes. The high intensity implies more anchoring groups that can bind effectively with the TiO_2 nanoparticles and increase the electrons transfer process between the dye extracts and TiO_2 layer, which increases short circuit current and power conversion efficiency of the DSSC [18, 26]. The extra vibrational peaks shown in Fig. 3b, located at ~ 2362 cm^{-1} in S:H-1:3 shows the presence of more N–H/C–O anchoring groups which increases the binding sites on the TiO_2 nanoparticles as compared to other dyes [27] and therefore, this mass ratio can serve as the optimum value for the performance of DSSCs in this investigation.

3.3 Photoluminescence spectra (PL) of un-adsorbed plant dyes

Photoluminescence is the emission of light when photons are absorbed by a material, in the process, the material absorbs a photon, generates electron–hole pairs, transitions it to higher energy level, and returns it to the lower level by emitting a photon. It is an important tool in the characterization of opto-electronic devices [2]. To gain

Fig. 3 a FTIR spectra for pumpkin leaf (P), sweet potato leaf (S), hibiscus flower (H), P:H-1:3 and S:H-1:3, b Enlarged spectra between 3000 and 2800 cm^{-1}.
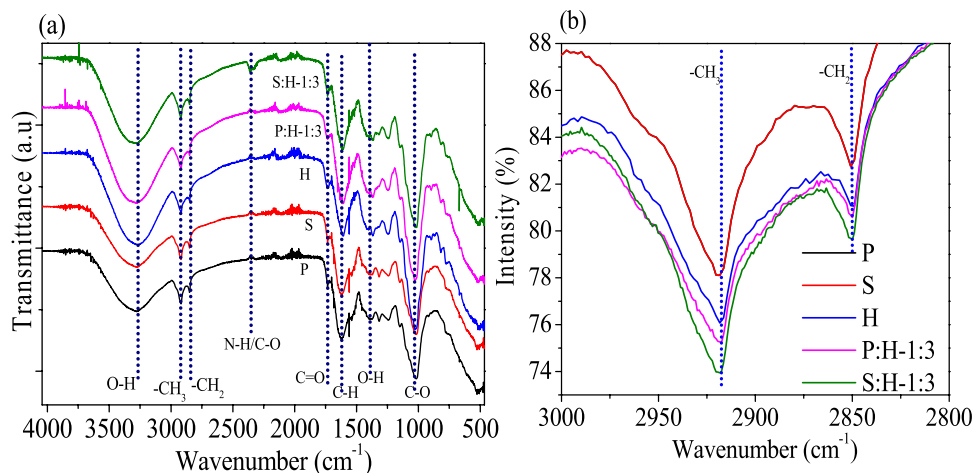
more insights between photoelectric conversion and photoemission, we probe the single and composite dye extracts with a 350 nm laser and record their photoemission properties as shown in Fig. 4. Figure 4a shows the PL spectra of sweet potato leaf powder. Three peaks were observed, a broad peak in the blue region with a maximum at 490 nm (2.53 eV), a sharp peak at 676 nm (1.83 eV) and an arm at 723 nm (1.72 eV). The arm at 723 nm is the characteristic of chlorophyll [2, 9]. No green emission was observed. Figure 4b shows the PL spectra for pumpkin leaf. The observed peaks have been explained in our previous work [2]. Figure 4c show the PL spectra of hibiscus flower with a broad peak in the UV–Visible spectrum and two distinct peaks corresponding to 462 nm (2.7 eV) and 620 nm (2.0 eV). These energy values are consistent with the UV–Vis absorption spectra. Figure 4d shows the PL spectra for the composites. The spectra have similar features corresponding to the single PL peaks for chlorophyll and anthocyanin except with enhanced intensity for SH in the red region of the spectrum. The peaks in the near red region of the spectrum originate from the recombination of a photo-generated hole with a singly ionized electron in the valence band and is responsible for red emission in materials [9].

3.4 Photoluminescence spectra (PL) of dye adsorbed on TiO$_2$ nanoparticles

To examine the photoemission of dyes adsorbed onto the TiO$_2$ nanoparticles, TiO$_2$ paste was deposited on soda lime glass substrate (SLG) by drop casting method following procedures reported elsewhere [2]. Figure 5 shows the PL spectra of individual and composite dye extracts adsorbed onto TiO$_2$ nanoparticles of particle size 12 ± 2nm [2]. For all the dye adsorbed on TiO$_2$, they have identical pattern in the UV region with a distinct peak positioned at ~450 nm. This peak emission positions are identical to those obtained from UV–visible spectroscopy. From Fig. 5a–e, generally, there is reduction in peak emission intensity for all the dye adsorbed samples and the total disappearance of the arm peak which was located 723 nm. Lower intensity suggests reduced electron–hole recombination rates and vice versa [9]. The composite dyes (S:H-1:3 & P:H-1:3) adsorbed on the TiO$_2$ nanoparticles have the lowest emission intensities suggesting lower electron–hole recombination rates and higher power conversion efficiencies [2, 9, 28–30].

3.5 Device J-V characterization

Figure 6a shows the photo-image of the fabricated solar cell device and Fig. 6b shows the set-up used for *J-V*
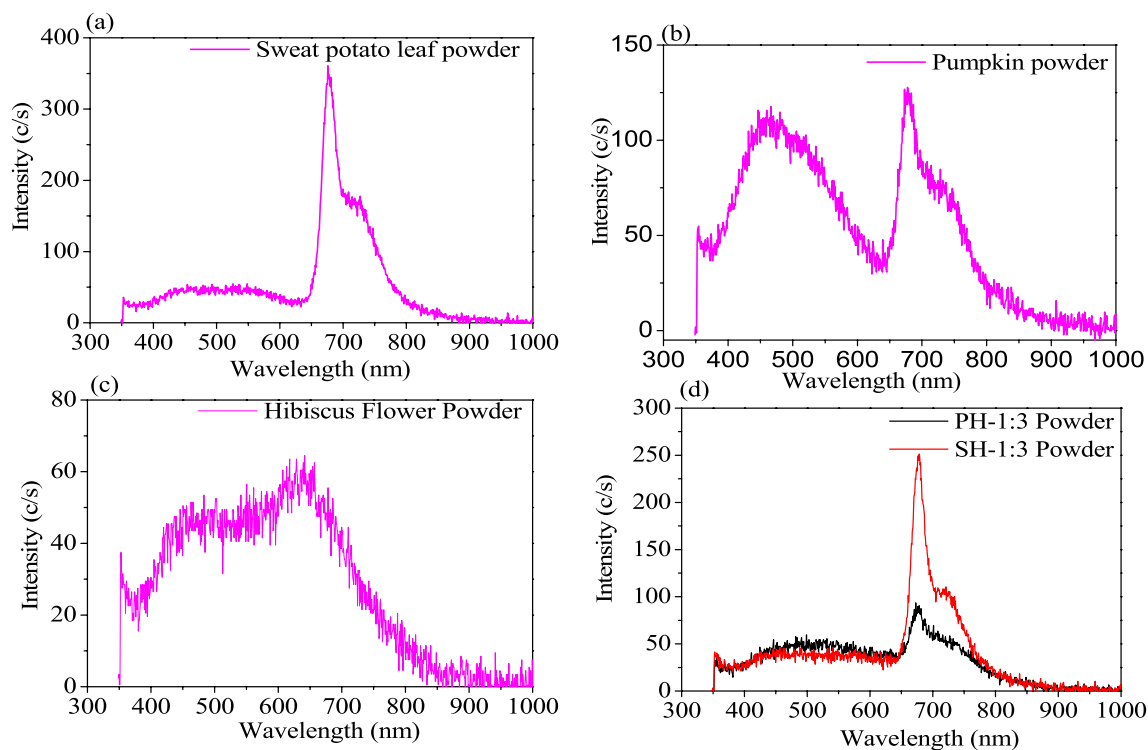

Fig. 4 PL spectra of powdered plant materials: **a** sweet potato leaf (S), **b** Pumpkin leaf (P), **c** Hibiscus flower (H) and **d** the composites in the ratios indicated (P:H-1:3 & S:H-1:3). Figure b is reproduced with permission from reference [2]
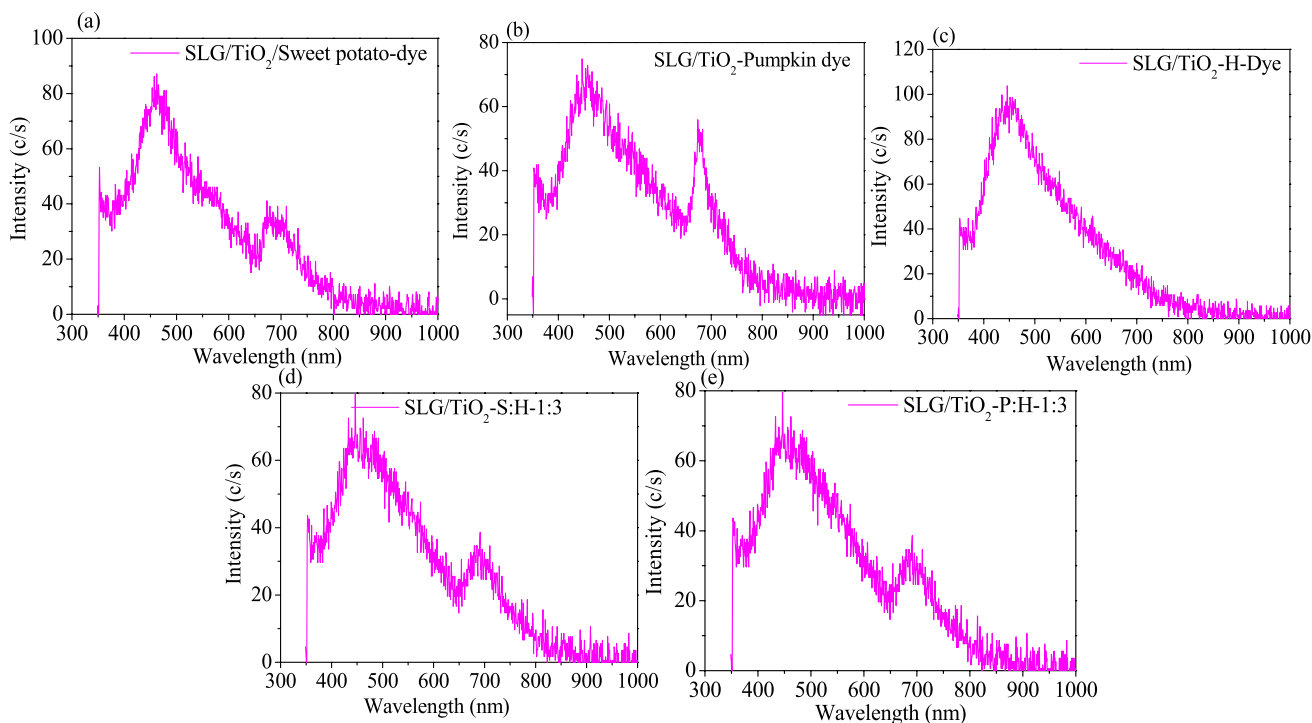
Fig. 5 a–e PL spectra of dyes adsorbed on TiO$_2$ nanoparticle taken after 30 days. The thin films were deposited on soda lime glass substrate (SLG)
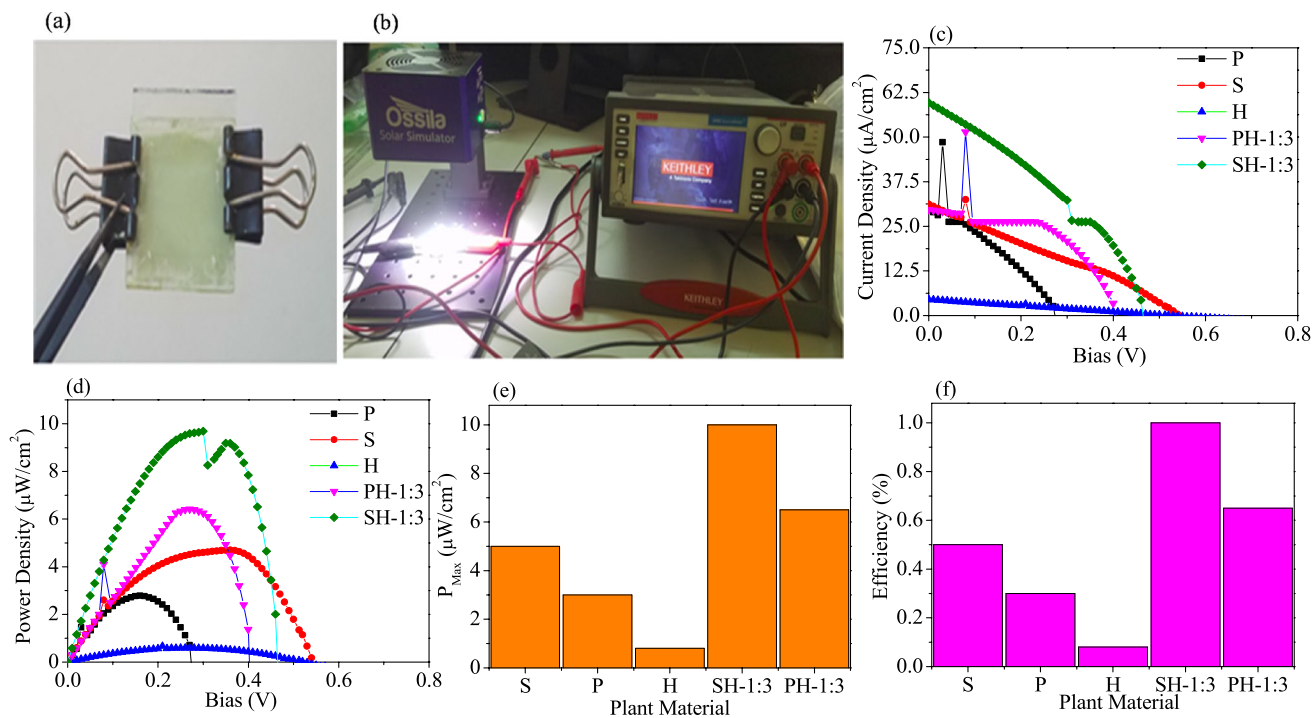

Fig. 6 a Optical image of fabricated DSSCs, **b** optical image of solar simulator, and Keithley SMU-2450, **c** *J-V* characteristics of the devices under 1 sun (i.e, $P_{incidence}$=100 mW/cm^2), **d** power density versus bias for the plant material's, **e** histogram of maximum power for the plant materials and **f** Histogram of efficiency of the different plant materials

measurements. Figure 6c shows the *J-V* characteristics of the DSSCs. The summary of the short circuit current and open circuit voltage is indicated in Table 1. Figure 6d shows a graph of power density against voltage. The material with the highest power density is the composite of S:H-1:3. From the table, it can be observed that hibiscus has the lowest short circuit current and the highest open circuit voltage, whereas the composite of S:H-1:3 has the highest short circuit current density, and maximum power density resulting into the highest power conversion efficiency of 1%. The variation of maximum power extracted from the devices and the power conversion efficiencies are illustrated in the histogram shown in Fig. 6e and f respectively.

The best power conversion efficiency in sweet potato single dye based DSSC is attributed to higher short circuit current density and reduction of electron–hole pair recombination's. Generally, as summarised in Table 1 and illustrated in the histograms, dye sensitized solar cells fabricated from dye composites have better power conversion efficiencies than the individual dyes. The cell based on SH dye composite has a power conversion efficiency of 1.0% which is greater than that of PH (0.65%) composite based DSSC. The highest efficiency observed in the S:H-1:3 composite is attributed to the wide range of optical absorption spectrum, reduction in defect states, reduced electron–hole pair recombination rates and the presence of a large number of C-H, CH_3, CH_2, N–H/C–O anchoring group that bind effectively on TiO_2 nanoparticles, thus increasing the short circuit current and power conversion efficiency of the DSSC. The performance of this new family of dyes is comparable and even better than previous studies as summarised in Table 1 [11, 14, 16, 19, 23–27].

3.6 Surface morphology of dye sensitized photo-anodes

A scanning electron microscope was used to determine the distribution of adsorbed dye extracts on the photoanodes. Figure 7a–e shows the surface morphology of H, P, S, P:H-1:3 and S:H-1:3 dyes adsorbed on TiO_2 nanoparticles respectively. It is observed that the single and composite dyes are fairly uniformly distributed across the entire photoanodes. The dyes are adsorbed on highly macroporous homogeneously distributed spherically shaped TiO_2 nanoparticles. The macroporosity is advantageous for good percolation of the electrolyte through the TiO_2 matrix and promotes continuous charge transport across the entire device structure [39, 40].

3.7 Device J-V stability experiments

To evaluate the stability of the device stored under ambient temperature conditions, the *J-V* measurements were carried after 7 and 30 days. The data were recorded and interpreted as shown in Figs. 8a–d and 9a–d for device *J–V* measurements taken after 7 and 30 days respectively. The device efficiencies are relatively stable with no significant dye degradation after 7 days. However, significant dye degradation occurred after 30 days which resulted into the device efficiencies being reduced to almost half.

4 Correlation between UV–Vis, FTIR and PL spectra on the device performance

The UV–Vis spectra provide the photon absorption wavelength range of the device. For Hibiscus, one prominent peak in the "blue" region of the spectrum was identified. Two prominent bands were identified in chlorophyll single based

Table 1 Photovoltaic parameters of the fabricated solar cells and literature values under 1 sun illumination

| S.n	Plant material	J_{sc} (mA/cm^2)	V_{oc} (V)	P_{max} (μW/cm^2)	FF	η (%)	References
1	Pumpkin leaf (P)	0.0303	0.28	3	–	0.30	This work
2	Sweet potato leaf (S)	0.0314	0.55	5	–	0.50	This work
3	Hibiscus flower (H)	0.0044	0.67	0.8	–	0.08	This work
4	P:H-1:3	0.0296	0.41	6.5	–	0.65	This work
5	S:H-1:3	0.0603	0.47	10	–	1.0	This work
6	Chrysanthemum (violet, green and blue)	0.34—0.85	0.47–0.58	–	0.41–0.48	0.485 – 1.35	[31]
7	Prickly Pear Fruit	2.64–3.49	0.61–0.66	–	0.47–0.61	0.75–1.4	[32]
8	Coral Gerbera, orange Gerbera, Red Gerbera, Yellow Gerbera	0.00–1.22	0.58–0.59	–	0.51–0.56	1.12–1.54	[25]
9	Blackberry, pomegranate, and black grape	0.82–6.69	0.35–1.18	–	0.3–0.45	0.39–1.05	[33]
10	Chlorophyll and anthocyanin Co-sensitizers	0.65–2.91	0.56–0.64	–	0.40–0.61	0.18–1.14	[13]
11	Serratia marcescens 11E (prodigiosin pigment)	0.096	0.56	–	0.597	0.032	[34]
12	Cassia fistula	0.54	0.51	–	0.65	0.21	[35]
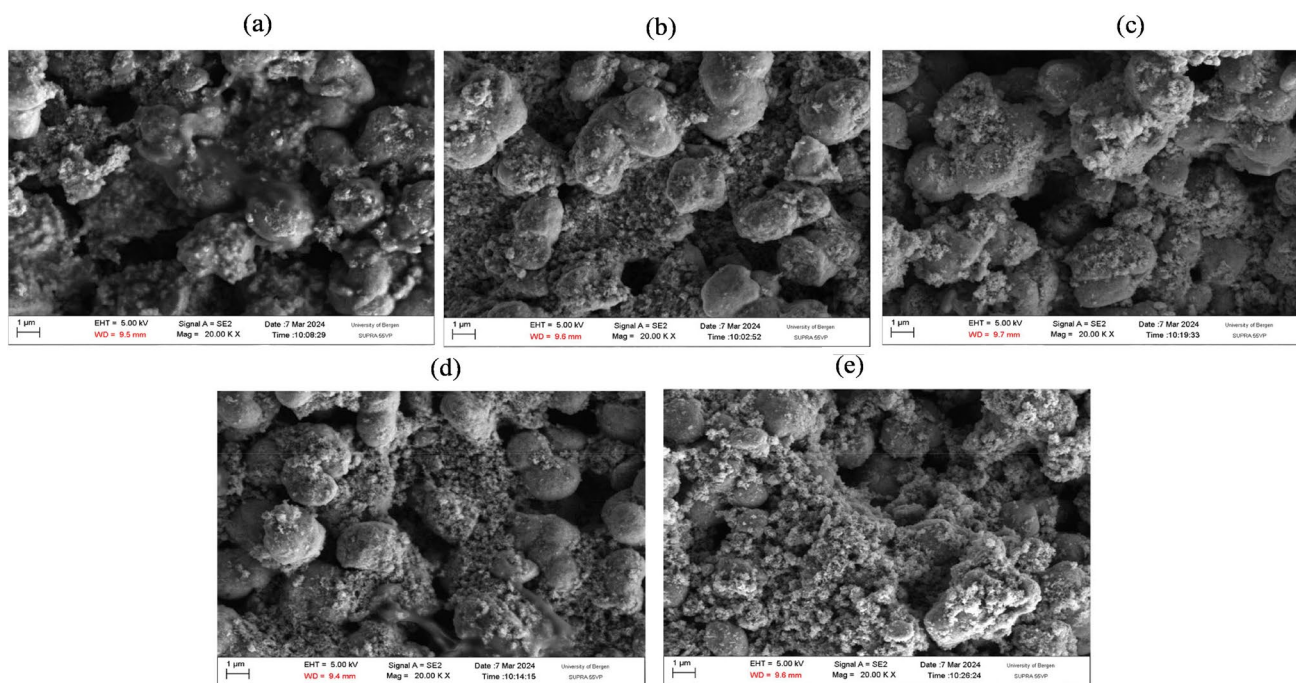
Fig. 7 SEM images of TiO$_2$ photo-anodes sensitized with; **a** P, **b** H, **c** S, **d** P:H-1:3 and **e** S:H-1:3 dye extracts.
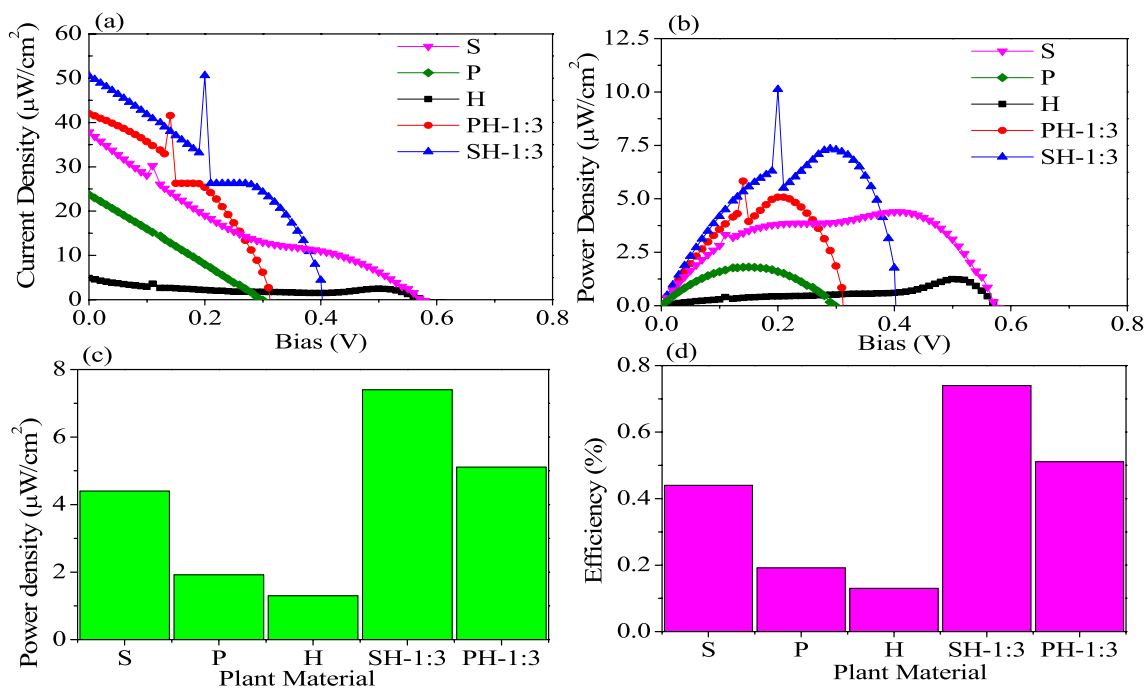

Fig. 8 a *J-V* characteristics of the devices under 1 sun (i.e, $P_{incidence}$=100 mW/cm^2), **b** power density versus bias for the plant material's, **c** histogram of maximum power for the plant materials and **d** histogram of efficiency of the different plant materials. Measurements were taken after seven days

dyes; the "blue" band and the "red" band, whereas for mixed dyes, the bands were across the entire spectrum with two prominent bands; the "blue" band and the "red" band. These

photon peaks in the entire UV–Vis–near infrared spectrum are responsible for the conversion of the sun's energy into electric power. The FTIR spectra provides the anchoring
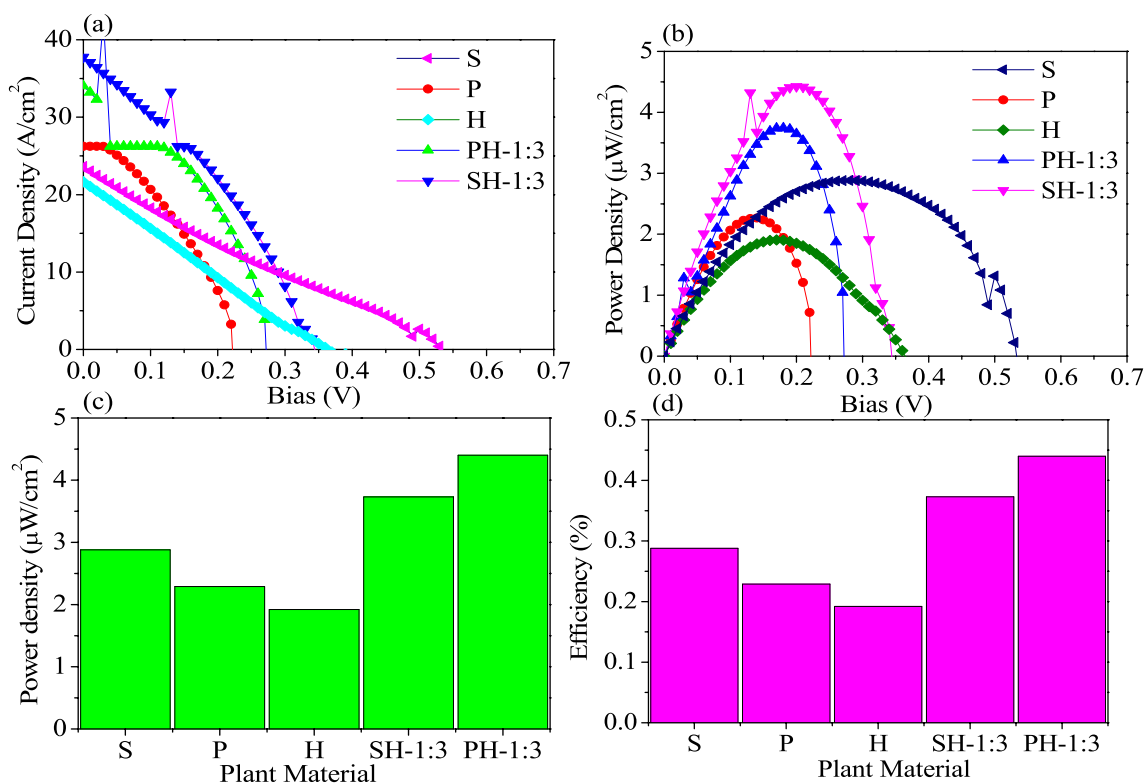
Fig. 9 a *J-V* characteristics of the devices under 1 sun (i.e, $P_{incidence}$=100 mW/cm^2), **b** power density versus bias for the plant material's, **c** histogram of maximum power for the plant materials and **d** histogram of efficiency of the different plant materials. Measurements were taken after 30 days

(functional) groups that bind effectively with the TiO$_2$ nanoparticles. This anchoring groups enables the charge transfer processes between the dye and the TiO$_2$ nanoparticles. The higher the number of anchoring groups, the higher the efficiency. The higher intensities observed in the FTIR spectra for the composites as compared to their single dye counter parts is due to the presence of a large number of anchoring groups on the surface of TiO$_2$ nanoparticles. For the same reason, the efficiencies of the DSSC with composites is higher than that of single dye extracts. The PL spectra provides the relationship between photon emission and photoelectric conversion of the dye sensitized solar cells. The higher the intensity of photon emission, the poor performance of the device. In this case, it has been observed that single dyes adsorbed onto TiO$_2$ nanoparticles have higher PL intensities and mixed dyes have lower PL intensities and thus higher power conversion efficiencies.

5 Conclusions

In summary, we have extracted chlorophyll and anthocyanin pigments and applied them as sensitizers and co-sensitizers in dye sensitized solar cells. The dyes absorb light in the UV–visible and near infrared region of the electromagnetic spectrum. Our findings show that dye composites have a synergetic effect on optical absorption properties and eventually enhancing the power conversion efficiency of the DSSC. In particular, five different solar cells with dye extract from hibiscus, pumpkin leaf, sweat potato leaf, and their two composites revealed a power conversion efficiency of ~ 0.08, 0.3, 0.5, 0.7 and 1%, respectively. The enhanced efficiency has been supported by a decrease in the photoluminescence emission spectra intensities for the adsorbed dyes onto TiO$_2$ nanoparticles and has been attributed to more O–H, C–C and C = O binding sites onto TiO$_2$ nanoparticles, reduced rate of electron–hole pair recombination and a wide wavelength range of optical absorption. The device efficiencies were reduced by half of the original value after 30 days, which makes their industrial applications and long term use unrealistic. Although the power conversion efficiency was improved by using this strategy, the reported efficiency is almost 13 times lower than that of the synthetic dyes. Strategies on stabilizing the dye and increasing the power conversion efficiency to match or better than those of synthetic dyes are areas that require further research.

Author contributions Emma Panzi Mukhokosi and Mohammed Tibenkana collected, prepared and analyzed the samples. Mohammed Tibenkana wrote the first draft of the manuscript. The final manuscript was read and approved by all authors.

Declarations

Conflict of interest The authors declare that there are no conflicts of interest/competing interests.

References

1. K.T. Butler, J.M. Frost, A. Walsh, Ferroelectric materials for solar energy conversion: photoferroics revisited. Energy Environ. Sci. **8**, 838–848 (2015). https://doi.org/10.1039/C4EE03523B

2. E.P. Mukhokosi, M. Maaza, M. Tibenkana, N.L. Botha, L. Namanya, I.G. Madiba, M. Okullo, Optical absorption and photoluminescence properties of Cucurbita maxima dye adsorption on TiO$_2$ nanoparticles. Mater. Res. Express. (2023). https://doi.org/10.1088/2053-1591/acce91

3. G. Calogero, A. Bartolotta, G. Di Marco, A. Di Carlo, F. Bonaccorso, Vegetable-based dye-sensitized solar cells. Chem. Soc. Rev. **44**, 3244–3294 (2015). https://doi.org/10.1039/c4cs00309h

4. A. Omar, H. Abdullah, Electron transport analysis in zinc oxide-based dye-sensitized solar cells: a review. Renew. Sustain. Energy Rev. **31**, 149–157 (2014). https://doi.org/10.1016/j.rser.2013.11.031

5. F.W. Low, C.W. Lai, Recent developments of graphene-TiO2 composite nanomaterials as efficient photoelectrodes in dye-sensitized solar cells: a review. Renew. Sustain. Energy Rev. **82**, 103–125 (2018). https://doi.org/10.1016/j.rser.2017.09.024

6. M. Grätzel, The light and shade of perovskite solar cells. Nat. Mater. **13**, 838–842 (2014). https://doi.org/10.1038/nmat4065

7. E. Singh, H.S. Nalwa, Graphene-based dye-sensitized solar cells: a review. Sci. Adv. Mater. **7**, 1863–1912 (2015). https://doi.org/10.1166/sam.2015.2438

8. V.M. Mwalukuku, J. Liotier, A.J. Riquelme, Y. Kervella, Q. Huaulmé, A. Haurez, S. Narbey, J.A. Anta, R. Demadrille, Strategies to improve the photochromic properties and photovoltaic performances of naphthopyran dyes in dye-sensitized solar cells. Adv. Energy Mater. (2023). https://doi.org/10.1002/aenm.202203651

9. A. Soosairaj, A. Gunasekaran, S. Anandan, L.R. Asirvatham, Synergetic effect of *Leucophyllum frutescens* and *Ehretia microphylla* dyes in enhancing the photovoltaic performance of dye-sensitized solar cells. Environ. Sci. Pollut. Res. (2023). https://doi.org/10.1007/s11356-023-26132-z

10. S.C. Yadav, M.K. Tiwari, A. Kanwade, H. Lee, A. Ogura, P.M. Shirage, Butea monosperma, crown of thorns, red lantana camara and royal poinciana flowers extract as natural dyes for dye sensitized solar cells with improved efficiency. Electrochim. Acta **441**, 141793 (2023). https://doi.org/10.1016/j.electacta.2022.141793

11. M. Shobana, P. Balraju, P. Senthil Kumar, N. Muthukumarasamy, R. Yuvakkumar, D. Velauthapillai, Investigation on the performance of nanostructure TiO$_2$ bi-layer as photoanode for dye sensitized solar cell application. Sustain. Energy Technol. Assessments. **52**, 102295 (2022). https://doi.org/10.1016/j.seta.2022.102295

12. M. Fallah, I. Maleki, M.R. Zamani-Meymian, Y. Abdi, Enhancing the efficiency of dye-sensitized solar cell by increasing the light trapping and decreasing the electron-hole recombination rate due to Ag@TiO$_2$ core-shell photoanode structure. Mater. Res. Express. (2019). https://doi.org/10.1088/2053-1591/ab5c8a

13. S.C. Ezike, C.N. Hyelnasinyi, M.A. Salawu, J.F. Wansah, A.N. Ossai, N.N. Agu, Synergestic effect of chlorophyll and anthocyanin co-sensitizers in TiO$_2$-based dye-sensitized solar cells. Surf. Interfaces. **22**, 100882 (2021). https://doi.org/10.1016/j.surfin.2020.100882

14. S. Sathyajothi, R. Jayavel, A.C. Dhanemozhi, The fabrication of natural dye sensitized solar cell (Dssc) based on TiO$_2$ using henna and beetroot dye extracts. Mater. Today Proc. **4**, 668–676 (2017). https://doi.org/10.1016/j.matpr.2017.01.071

15. Y. Yuniati, P.E. Elim, R. Alfanaar, H.S. Kusuma, Mahfud, Extraction of anthocyanin pigment from hibiscus sabdariffa l. By ultrasonic-assisted extraction. IOP Conf. Ser. Mater. Sci. Eng. (2021). https://doi.org/10.1088/1757-899X/1010/1/012032

16. M.R. Munandar, A.S.R. Hakim, H.A. Puspitadindha, S.P. Andiyani, F. Nurosyid, The effect of mixing Chlorophyll-Antocyanin as a natural source dye on the efficiency of dye-sensitized solar cell (DSSC). J. Phys. Conf. Ser. (2022). https://doi.org/10.1088/1742-6596/2190/1/012042

17. Hardeli, R. Zainul, L.P. Isara, Preparation of dye sensitized solar cell (DSSC) using anthocyanin color dyes from jengkol shell (Pithecellobium lobatum Benth.) by the gallate acid copigmentation. J. Phys. Conf. Ser. (2019). https://doi.org/10.1088/1742-6596/1185/1/012021

18. N. Chaudhri, N. Sawhney, B. Madhusudhan, A. Raghav, M. Sankar, S. Satapathi, Effect of functional groups on sensitization of dye-sensitized solar cells (DSSCs) using free base porphyrins. J. Porphyr. Phthalocyanines. **21**, 222–230 (2017). https://doi.org/10.1142/S1088424617500390

19. A.K. Rajan, L. Cindrella, Studies on new natural dye sensitizers from Indigofera tinctoria in dye-sensitized solar cells. Opt. Mater. (Amst) **88**, 39–47 (2019). https://doi.org/10.1016/j.optmat.2018.11.016

20. S.M. Milenković, J.B. Zvezdanović, T.D. Andelković, D.Z. Marković, The identification of chlorophyll and its derivatives in the pigment mixtures: HPLC-chromatography, visible and mass spectroscopy studies. Adv. Technol. **1** (2012) 16–24. http://alfa.tf.ni.ac.rs/casopis/sveska1/c2.pdf.

21. S. Alhorani, S. Kumar, M. Genwa, P.L. Meena, Performance of dye-sensitized solar cells extracted dye from wood apple leaves. J. Phys. Commun. (2022). https://doi.org/10.1088/2399-6528/ac8785

22. K. Sharma, V. Sharma, S.S. Sharma, Dye-sensitized solar cells: fundamentals and current status. Nanoscale Res. Lett. (2018). https://doi.org/10.1186/s11671-018-2760-6

23. K.C. Cho, H. Chang, C.H. Chen, M.J. Kao, X.R. Lai, A study of mixed vegetable dyes with different extraction concentrations for use as a sensitizer for dye-sensitized solar cells. Int. J. Photoenergy (2014). https://doi.org/10.1155/2014/492747

24. S. Ananth, P. Vivek, G. Saravana Kumar, P. Murugakoothan, Performance of *Caesalpinia sappan* heartwood extract as photo sensitizer for dye sensitized solar cells, Spectrochim. Acta- Part A Mol. Biomol. Spectrosc. **137**, 345–350 (2015). https://doi.org/10.1016/j.saa.2014.08.083

25. F.M.M. dos Santos, A.M.B. Leite, L.R.B. da Conceição, Y. Sasikumar, R. Atchudan, M.F. Pinto, R. Suresh Babu, A.L.F. de Barros, Effect of bandgap energies by various color petals of Gerbera jamesonii flower dyes as a photosensitizer on enhancing

the efficiency of dye-sensitized solar cells. J. Mater. Sci. Mater. Electron. **33**, 20338–20352 (2022). https://doi.org/10.1007/s10854-022-08849-8

26. S. Alhorani, S. Kumar, M. Genwa, P.L. Meena, Dye extracted from Bael leaves as a photosensitizer in dye sensitized solar cell. Mater. Res. Express. (2021). https://doi.org/10.1088/2053-1591/ac3aa7

27. V.R. Netala, V.S. Kotakadi, V. Nagam, P. Bobbu, S.B. Ghosh, V. Tartte, First report of biomimetic synthesis of silver nanoparticles using aqueous callus extract of Centella asiatica and their antimicrobial activity. Appl. Nanosci. **5**, 801–807 (2015). https://doi.org/10.1007/s13204-014-0374-6

28. H.L. Hao, W.S. Wu, Y. Zhang, L.K. Wu, W.Z. Shen, Origin of blue photoluminescence from colloidal silicon nanocrystals fabricated by femtosecond laser ablation in solution. Nanotechnology (2016). https://doi.org/10.1088/0957-4484/27/32/325702

29. W.S. Wu, H.L. Hao, Y.X. Zhang, J. Li, J.J. Wang, W.Z. Shen, Correlation between luminescence and structural evolution of colloidal silicon nanocrystals synthesized under different laser fluences. Nanotechnology **29**, 025709 (2018). https://doi.org/10.1088/1361-6528/aa95a1

30. Y. Lin, G. Lin, B. Sun, X. Guo, Nanocrystalline perovskite hybrid photodetectors with high performance in almost every figure of merit. Adv. Funct. Mater. **28**, 1–11 (2018). https://doi.org/10.1002/adfm.201705589

31. A.M.B. Leite, H.O. da Cunha, A.F.C.R. Rodrigues, R. Suresh Babu, A.L.F. de Barros, Construction and characterization of organic photovoltaic cells sensitized by Chrysanthemum based natural dye, Spectrochim. Acta- Part A Mol. Biomol. Spectrosc. **284**, 121780 (2023). https://doi.org/10.1016/j.saa.2022.121780

32. R. Rajendhiran, R. Atchudan, J. Palanisamy, A. Balasankar, T.H. Oh, V. Deivasigamani, S. Ramasundaram, Prickly pear fruit extract: capping agent for the sol-gel synthesis of discrete titanium dioxide nanoparticles and sensitizer for dye-sensitized solar cell. Coatings **13**, 579 (2023). https://doi.org/10.3390/coatings13030579

33. I.S. Mohamad, M.N. Norizan, N. Mahmed, N. Jamalullail, D.S.C. Halin, M.A.A.M. Salleh, A.V. Sandu, M.S. Baltatu, P. Vizureanu, Enhancement of power conversion efficiency with zinc oxide as photoanode and cyanococcus, *Punica granatum* L., and *Vitis vinifera* as natural fruit dyes for dye-sensitized solar cells. Coatings (2022). https://doi.org/10.3390/coatings12111781

34. P. Hernández-Velasco, I. Morales-Atilano, M. Rodríguez-Delgado, J.M. Rodríguez-Delgado, D. Luna-Moreno, F.G. Ávalos-Alanís, J.F. Villarreal-Chiu, Photoelectric evaluation of dye-sensitized solar cells based on prodigiosin pigment derived from *Serratia marcescens* 11E. Dye. Pigment. (2020). https://doi.org/10.1016/j.dyepig.2020.108278

35. I. Chandra Maurya, S. Singh, P. Srivastava, B. Maiti, L. Bahadur, Natural dye extract from Cassia fistula and its application in dye-sensitized solar cell: experimental and density functional theory studies. Opt. Mater. (Amst). **90**, 273–280 (2019). https://doi.org/10.1016/j.optmat.2019.02.037

36. S.A. Mahadik, H.M. Yadav, S.S. Mahadik, Surface properties of chlorophyll-a sensitized TiO_2 nanorods for dye-sensitized solar cells applications. Colloids Interface Sci. Commun. **46**, 100558 (2022). https://doi.org/10.1016/j.colcom.2021.100558

37. O. Adedokun, O.L. Adedeji, I.T. Bello, M.K. Awodele, A.O. Awodugba, Fruit peels pigment extracts as a photosensitizer in ZnO-based dye-sensitized solar cells. Chem. Phys. Impact. **3**, 100039 (2021). https://doi.org/10.1016/j.chphi.2021.100039

38. N.Y. Amogne, D.W. Ayele, Y.A. Tsigie, Recent advances in anthocyanin dyes extracted from plants for dye sensitized solar cell. Mater. Renew. Sustain. Energy **9**, 1–16 (2020). https://doi.org/10.1007/s40243-020-00183-5

39. S. Ahmed, A. Du Pasquier, T. Asefa, D.P. Birnie, Improving microstructured TiO_2 photoanodes for dye sensitized solar cells by simple surface treatment. Adv. Energy Mater. **1**, 879–887 (2011). https://doi.org/10.1002/aenm.201100121

40. M.K. Hossain, M.F. Pervez, M.N.H. Mia, A.A. Mortuza, M.S. Rahaman, M.R. Karim, J.M.M. Islam, F. Ahmed, M.A. Khan, Effect of dye extracting solvents and sensitization time on photovoltaic performance of natural dye sensitized solar cells. Results Phys. **7**, 1516–1523 (2017). https://doi.org/10.1016/j.rinp.2017.04.011